

# METHOD AND ALGORITHMS FOR CASCADE CLASSIFICATION OF SULFUR PRINT IMAGES OF BILLET TRANSVERSE TEMPLATES

*I.A. Posokhov*<sup>1</sup>, posohoff@bk.ru,  
*O.S. Logunova*<sup>1</sup>, logunova66@gmail.com,  
*A.Yu. Mikov*<sup>1</sup>, mikov.ayu@gmail.com.

<sup>1</sup> Nosov Magnitogorsk State Technical University, Magnitogorsk, Russian Federation

This paper presents studies of sulfur print images of continuous cast billet transverse templates. The authors determined a problem of low reliability of information about the quality of billets. When assessing an image visually, such assessment is subjective with a human factor to a large extent. The authors developed a control point layout chart to collect graphical information in the course of casting billets. It is proposed to introduce three classes of images broken up by a template brightness/foreground ratio. Regarding an increased complexity of algorithms, the authors proposed the cascade classification of images. The technique includes assessment of images by shape-generating parameters of a histogram, by a distance to reference normed histograms, and by applying fuzzy logic methods. Experimental performance of the cascade technique showed that a simplified technique by assessing shape-generating parameters had expressly identified 22% of all images, by assessing a distance to reference normed histograms – 70% of the rest, and only by applying fuzzy logic methods all the rest images had been unambiguously identified. A 100% success of the classification is achieved only when applying all cascades of the developed technique.

*Keywords: sulfur print images; image histogram; shape-generating parameters; distance between objects; object identification rules; cascade classification.*

## Introduction

This paper focuses on an increase in reliability of a classification of steel billet sulfur print images. A sulfur print is an image produced during the industrial process and used to make a visual evaluation of the steel quality. Such visual examination entails an expert evaluation highly influenced by a human factor and decreased reliability of information about the quality. Received data are transferred to a steelmaking control system. In the earlier studies [1], the authors proposed an automatic system for intelligent support of continuous cast billet production control processes by processing graphical data of sulfur prints [2, 3].

Management of facilities and processes in modern conditions is characterized by rapid changes in external environment, including economic, social, scientific, and industrial areas. Innovative technologies in the industry require increased response and quality of decisions made on possible options of system creation and modification in the context of definite and ambiguous information. Available data processing methods use numerical, text, and graphical data in decision-making systems. Making decisions based on graphical data is the most complicated task. It is complicated due to preliminary processing stages which precede image segmentation and recognition [1].

Automatic segmentation of an original image showed that standard classification algorithms were sensitive to the image quality. Errors in segmentation may be eliminated

by preliminary processing of images depending on their properties. The authors propose to carry out image preliminary processing following an individual route which is determined subject to a class of such image.

There is current active research on classification of images and objects included in a structure of such images. Well-known solutions include results of work carried out in many countries of the world, including Russia.

One of approaches to the classification is to create a library of images by categories. For example, the paper [4] studied seven categories of images to build a vector classification system. The paper contains a theory of choice with linearly separable objects in an optimal hyperplane. The authors performed over 2670 tests with classes: *airplanes, birds, boats, buildings, fish, people, vehicles*. The authors applied in their studies the Gaussian distribution, the vector Laplace operator, and distribution  $\chi^2$  as a kernel. When building a classifier, the authors achieved a classification accuracy of 11-16%. The authors [5] propose to apply Support Vector Machines (SVM) for multiclass image classification. The paper contains a method of choice of hyperplanes. However, the authors state problems with applying methods, if a number of hyperplanes increase. The method was tested in a sphere of image recognition on an agricultural map of the East of England to determine fields with single-type crops. Examples of given images determine objects of a regular form.

Quite many papers focus on recognition of a human face and its elements. It is proposed to use automatic classification based on saliency maps. For example, the paper [6] proposes to use a 2D wavelet representation based on a plane wave restricted by an envelope to specify key points on the face. This method showed a peak generalization rate of 82%. Drawbacks of such method are sensitivity to the image quality and changes in a facial expression of key elements.

One of classification methods is determination of distinguished points of a pre-set texture [7, 8]. The paper [4] proposes an approximate basic model of image segmentation based on a point brightness evaluation. The authors of the paper applied an algorithm for brain images. As a result, accuracy of classification of images with various textures was up to 84,4%. The paper [8] deals with a statistical approach to classification of textures from separate images, which is based on determination of the quality of lighting, positions of cameras and image processing conditions. The method is based on the use of filters resistant to image rotation, evaluations of image histograms and forms of histograms. Decisions on an image class are made by applying the k-Means procedure which is sensitive to a choice of original cluster centers. The number of correctly classified textures for samples was 98%.

The task of image classification was also fulfilled by applying fuzzy sets and fuzzy logic. First papers on fuzzy sets applied to classification of images were published in the late 1980s and early 1990s and showed good results of recognition of cartographic representations with objects of a regular form [9, 10, 11].

Outlined fundamentals were developed in modern studies [12, 13, 14, 15, 16, 17]. However, in spite of many available studies, problems of classification of images with many objects of a non-regular form, low contrast ratio, low quality and contract ratio remain unsettled.

The above problems determined an objective of the research: increase in efficiency of operation of multi-stage metallurgical facilities based on human actions taken as a result of processing and analysis of graphical information about the quality of continuous cast billets. To achieve the objective, the research tasks have been completed:

1. **An information-theoretic analysis** of a multi-stage metallurgical process as a complex system and determination of a role of graphical information in the steel products quality assessment system.
2. Development **of an adaptive technique of cascade classification of graphical information** about the quality of continuous cast billets, including evaluation of shape-generating parameters of brightness histograms, a degree of similarity with reference histograms and position of the fuzzy set theory.
3. Design and development of a **decision-making system regarding identification of objects of a non-regular form in images** of continuous cast billet sulfur prints, including algorithms and software to process and visualize graphical information.
4. **Computational experiment to evaluate sensitivity and reliability** of the classification technique and the decision-making system in industrial environment.

As part of this paper, the authors state how the second task is completed.

A subject of the research is sulfur print images produced at a quality control stage of continuous cast billets when they are transferred from continuous casting to metal forming. A scope of the research is software of the decision-making system regarding the quality of billets based on segmentation of sulfur print images.

## 1. Methods

### 1.1. Acquisition of Sulfur Print Images

Regarding a typical steelmaking technology applied at iron and steel plants, we may specify three key points of graphical data collection and control in production divisions (see Fig. 1).

The point "Raw materials control" is set at the exit from the preparation division or at the entry to a group of steelmaking shops. For example, at burden material preparation sections. Functions of the point "Raw materials control" include evaluation of a grain-size composition of materials charged into steelmaking facilities: a fraction and type of scrap, a grain-size composition of bulk materials, etc. The results are used to predict an apparent density of materials, chemical composition of original burden and produced steel. Examples of images of burden materials are given in Fig. 2.

The point "Semi-finished products control" is set at the exit of billets from continuous casting machines. This point includes two stages: taking templates of billets directly on the industrial line; evaluations of development of internal and surface defects of the billet on the industrial section and in a special laboratory. Gained information is transferred to a technology control analytical laboratory to analyze operating modes of the caster. An example of the image of template sulfur print is given in Fig. 2c.

The point "Finished products control" is set in rolling shops after main stages of treatment. Control should be carried out in real time as sheets pass control sections or upon completion of production. Finished products quality control at the end of a complete production line requires extra costs for recoiling of every coil, personnel training, and delays output of a finished lot of products for a period of such examination. The fact of a subjective evaluation of the quality remains unchanged. Fig. 2d shows a segment of a cold rolled sheet containing a surface defect.

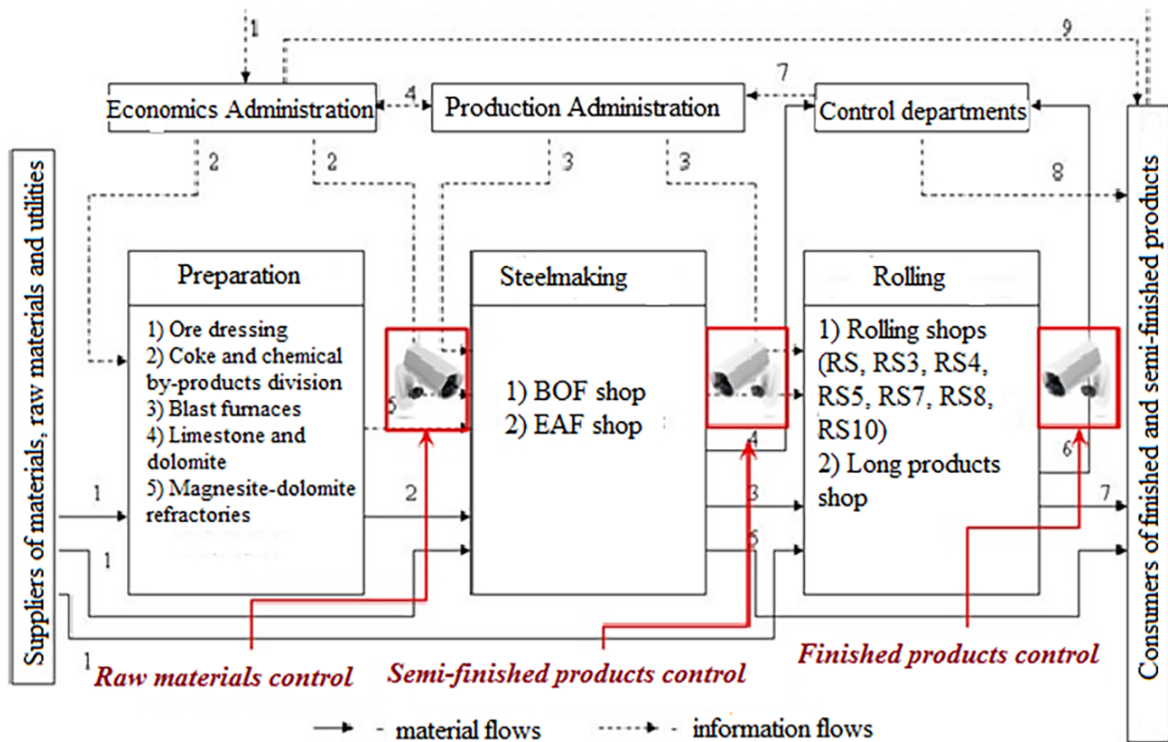
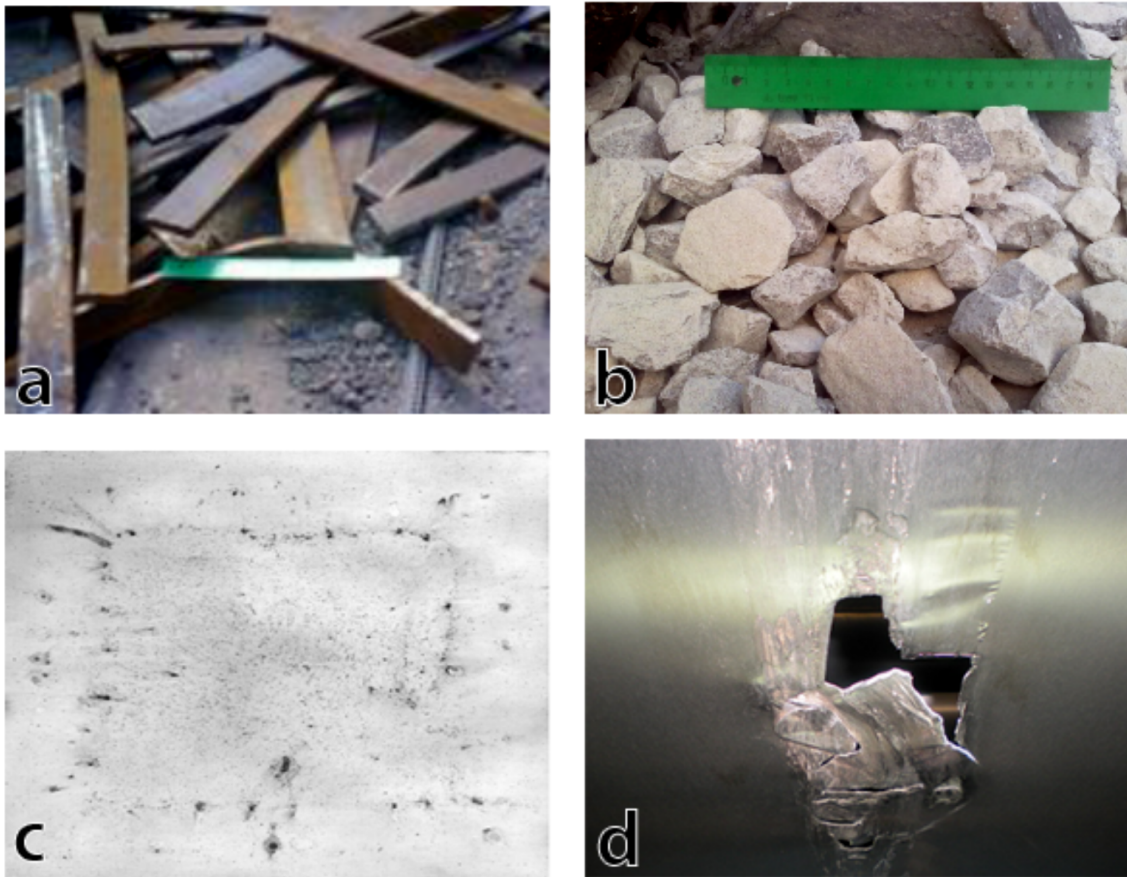


Fig. 1. Quality control points in an enlarged flow chart of the iron and steel works: BOF – basic oxygen furnace, EAF – electric arc furnace

Thus, graphical data are an integral part of characteristics of metallurgical products. When analyzing technologies, conditions of metallurgical equipment, and products quality, such data contribute to reliability, accuracy, and completeness of information support of the corporate management system.

One of techniques to control a continuous cast billet macrostructure is a visual evaluation of transverse templates and their sulfur prints. Templates are taken on a continuous steel casting section in an industrial steelmaking shop. Templates are delivered to the laboratory within 30 minutes after being taken to prepare sulfur prints. Sulfur prints are made by the Baumann method under GOST 10243-75. The manufacturing technique includes the following steps:

1. Preliminary treatment of a sample, grinding, polishing, cleaning from dust and grease spots.
2. Preparation of photographic paper, including wetting of sheets of photographic paper in a solution of 5% sulfuric acid for 5-8 minutes in the light and further drying to remove extra solution with filter paper.
3. Making prints by applying photographic paper on a template surface with an emulsion side, excluding its shifting, and flattening of photographic paper with a rubber roller to fully eliminate gas bubbles.
4. Thorough rinsing of finished prints in running water, processing with a fixer, rinsing, drying, and marking.



**Fig. 2.** Examples of images of burden materials and steel products: a – a segment of the picture of scrap; b – a segment of the picture of limestone  $CaCO_3$ ; c – internal defects of a continuous cast billet; d – a surface defect of cold rolled sheet

Prints are made at approx.  $20^{\circ}C$  during 3-15 minutes depending on steel alloying and sulfur content. Prints are considered to be ready, if photographic paper darkens from light brown to dark brown. Finished sulfur prints represent images with a size of about  $175 \times 230$  mm. By scanning sulfur prints, we make their electronic images. The size of the sulfur print does not exceed A4 format, therefore, we may use an A4, 300 dpi scanner. Scanned images have a resolution of about  $2100 \times 2800$  dots at the specified parameters. Examples of images corresponding to template sulfur prints scanned with a resolution of 300 dpi are given in Fig. 3.

When conducting a first set of an industrial experimental survey, we collected and studied 32 sulfur print images and retrospective information gained from heat logs. Having visually examined the group of images, we put forward a hypothesis that such group may be divided into three classes:

- class A: images containing a minor contrast between foreground brightness and the object under study;
- class B: images containing a medium contrast between foreground brightness and the object under study;

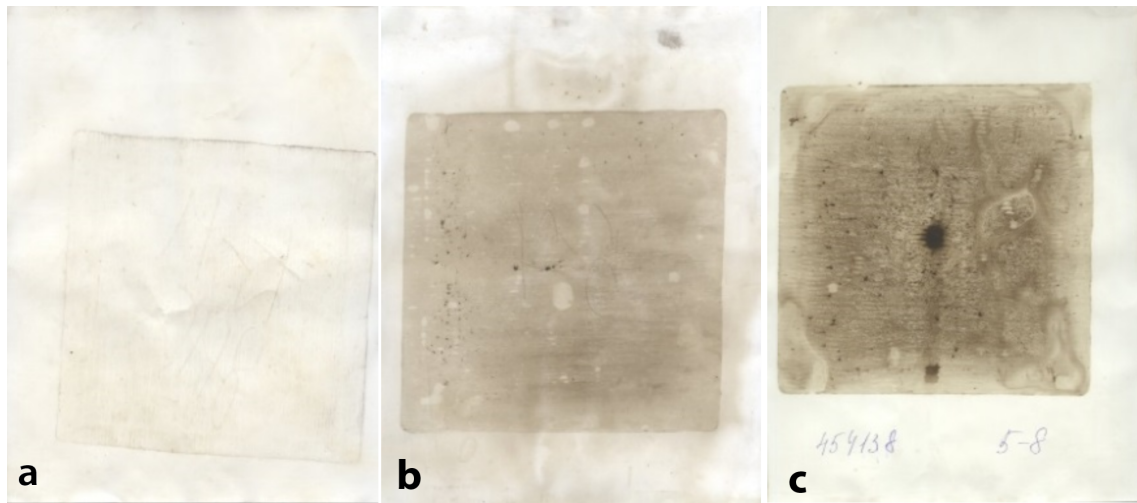


**Fig. 3.** Sulfur prints of transverse templates of continuous cast square billets

- class C: images containing a sharp contrast between foreground brightness and the object under study.

A visual analysis of the sulfur prints revealed features of images:

1. A sulfur print image always contains the object under study (the particular image of a transverse section of billets with a size of  $100 \times 100$  mm or  $150 \times 170$  mm) and surrounding background (see Fig. 4a).
2. A position of the transverse section of the object under study is indefinite and its coordinates cannot be simulated by known methods (see Fig. 4b).
3. Images are divided into three classes in view of brightness of the object under study and image background (see Fig. 4c).
4. A position of the transverse section of the object under study is indefinite and its coordinates cannot be simulated by known methods (see Fig. 4b).
5. Images are divided into three classes in view of brightness of the object under study and image background (see Fig. 4c).

Typical images of every class in increasing order of such ratio are given in Fig. 4.

In Fig. 4 number 1 specifies the background, number 2 – the object under study. As the image of the template is located in a part of the image only and its position is not definite, it was resolved to develop an algorithm of searching for an image area in an area of the sulfur print containing the object under study.

Original raster images of sulfur prints are full-color and represented in the RGB color model. In this model every color is represented with red, green and blue primary colors (components). A color of every dot of the image (pixel) is a result of mixing three components. The total number of bits used to represent every pixel in an RGB color space is called the color depth. The color depth of original images is 24 bits, i.e. every component (red, green, blue) has 8 bits. A total number of all possible colors of a 24-bit RGB image is  $(2^8)^3 = 16777216$ .

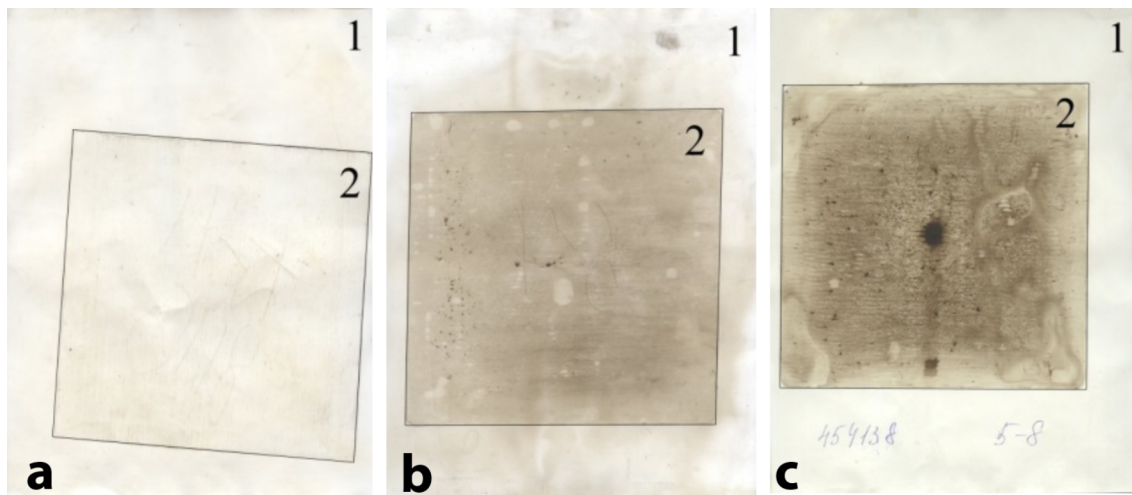


**Fig. 4.** Structure of images under study in terms "Object under study – background": a – a typical image of class A; b – a typical image of class B; c – a typical image of class C

Original images are processed into gray-scale ones with a color depth of 8 bits per pixel. In the context of the paper gray-scale images mean images in shades of gray. Every pixel of the image contains information about depth (brightness). A total number of possible gray gradations for an 8-bit gray-scale image is  $2^8 = 256$ . Minimum brightness (0) refers to black, maximum (255) – white.

Fig. 5 shows results of processing original images into gray-scale ones.

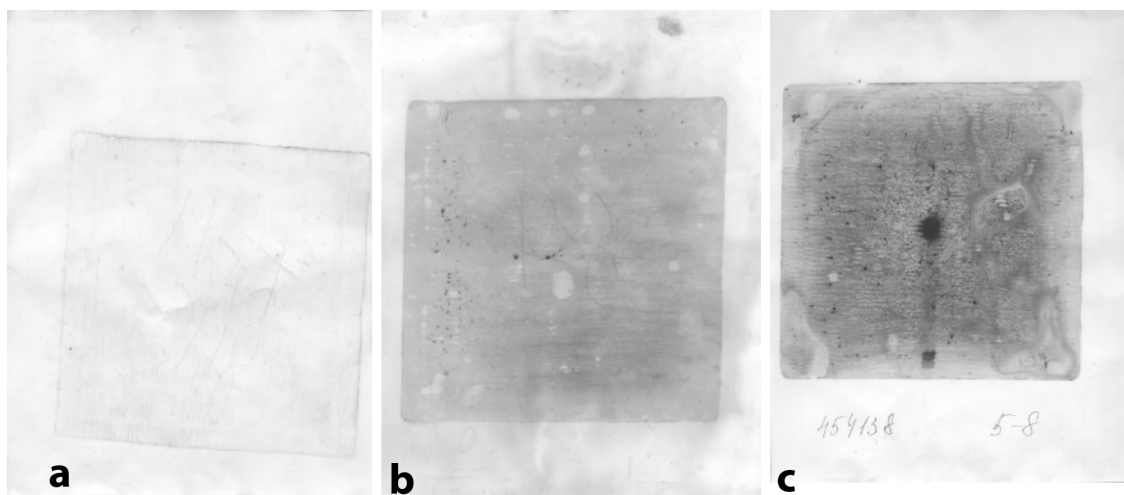


**Fig. 5.** Gray-scale images of sulfur prints of transverse templates of continuous cast square billets: a – a typical image of class A; b – a typical image of class B; c – a typical image of class C

A main strategy of converting full-color images into gray-scale ones is to apply photometry principles to compare brightness of the image in shades of gray and the original color image [18]. Brightness of a resulting pixel is calculated as a weighted sum of depth values of three RGB model components. Weights of color components are selected under ITU-R BT.709, which factors into features of human perception, higher sensitivity to green

and less to blue:

$$Y = 0.2126R + 0.7152G + 0.0722B,$$

where  $Y$  – brightness of a resulting pixel;  $R$ ,  $G$ ,  $B$  – color components of a pixel of the original image [19].

A block diagram of an algorithm for converting full-color images into gray-scale ones is given in Fig. 6. In Fig. 6 block 1 is used to initialize data, and then a 2D array of relevant values of pixel colors is uploaded into memory and its height and width are calculated. Block 2 organizes a cycle structure for every row of the array of pixels, block 3 – for every pixel. Any algorithm for converting full-color images into gray-scale ones is based on three actions:

- acquisition of values of red, green, and blue components of the pixel – block 4;
- calculation of brightness of a resulting pixel as a weighted sum of pixel components – block 5;
- assignment of calculated brightness to a pixel of the resulting image – block 6.

The algorithm results in a gray-scale image, whose size is the same as an original one, with a color depth of 8 bits per pixel.

## 1.2. A Technique to Classify Sulfur Print Images on the Basis of Shape-Generating Parameters of a Brightness Histogram

All sets of images made in the first series of the experimental survey are divided into three groups shown in Fig. 3. A key characteristic of the image is the brightness histogram.

The digital image brightness histogram is referred to as a discrete function:

$$h(r_k) = n_k,$$

where  $r_k$  – the  $k$ -th degree of brightness;  $n_k$  – number of image pixels with the brightness  $r_k$  [20]. For an 8-bit image  $k$  changes within limits  $[0; 255]$ . To determine which one of three supposed classes is attributed to the histogram, we introduce a term of shape-generating parameters of the histogram.

The shape-generating parameters of the histogram include the following:

- position of a brightness threshold –  $T$ ;
- position of brightness maximum to the left of the threshold –  $m$ ;
- position of brightness maximum to the right of the threshold –  $M$ ;
- value of the brightness function in each of specified points  $F(m)$ ,  $F(T)$  and  $F(M)$  (see Fig. 7).

To determine a brightness threshold value, we used algorithms given in [20, 21, 22, 23, 24]. According to these sources, a threshold value is a brightness value with respect to which the histogram is divided into two parts.

By dividing the histogram into two parts, we find brightness maximum of each part. The brightness threshold value is found by the Otsu method [23]. This method divides

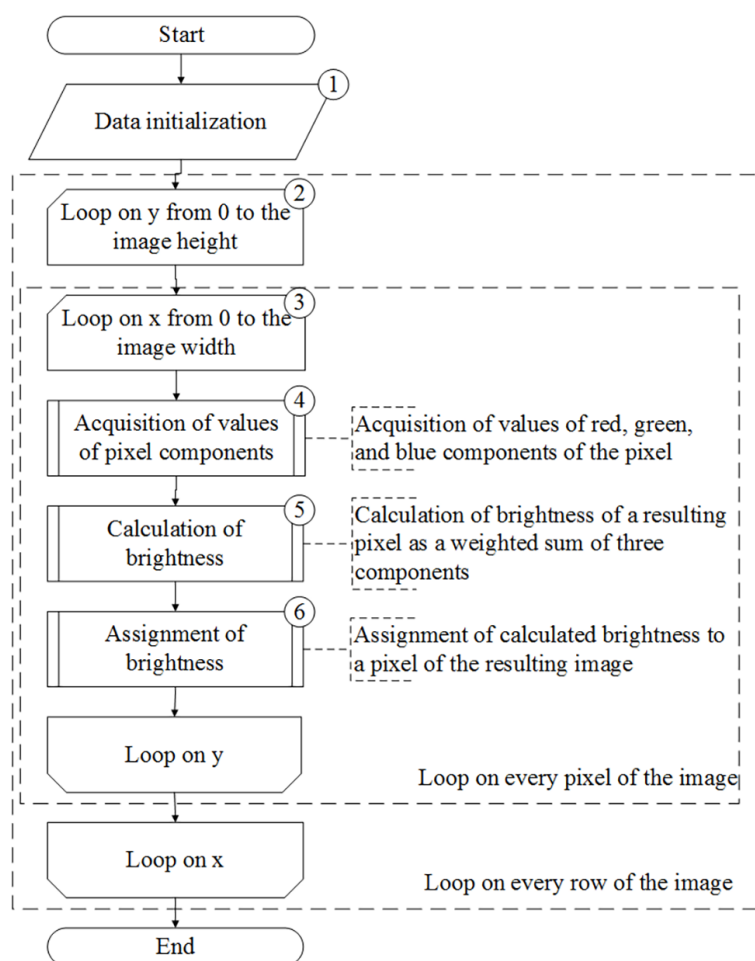


**Fig. 6.** A block diagram for converting full-color images into gray-scale ones

image pixels into two classes calculating a threshold so that an intraclass variance is minimum. Such variance is calculated as a weighted sum of variance of two classes:

$$\sigma_w^2(t) = \omega_1(t)\sigma_1^2(t) + \omega_2(t)\sigma_2^2(t),$$

where weights  $\omega_i$  – probabilities of two classes divided by the threshold  $t$ ;  $\sigma_i^2$  – variance of these classes.

The probability for each level of brightness is calculated as:

$$p(t) = \frac{n(t)}{N},$$

where  $n(t)$  – number of image pixels with the brightness  $t$ ;  $N$  – a total number of image pixels.

The author of the method [23] proved that minimization of the intraclass variance is equal to maximization of the interclass variance:

$$\sigma_b^2 = \sigma^2 - \sigma_w^2(t) = \omega_1(t)\omega_2(t) [\mu_1(t) - \mu_2(t)]^2,$$

where  $\mu_i$  – arithmetic mean of the class.

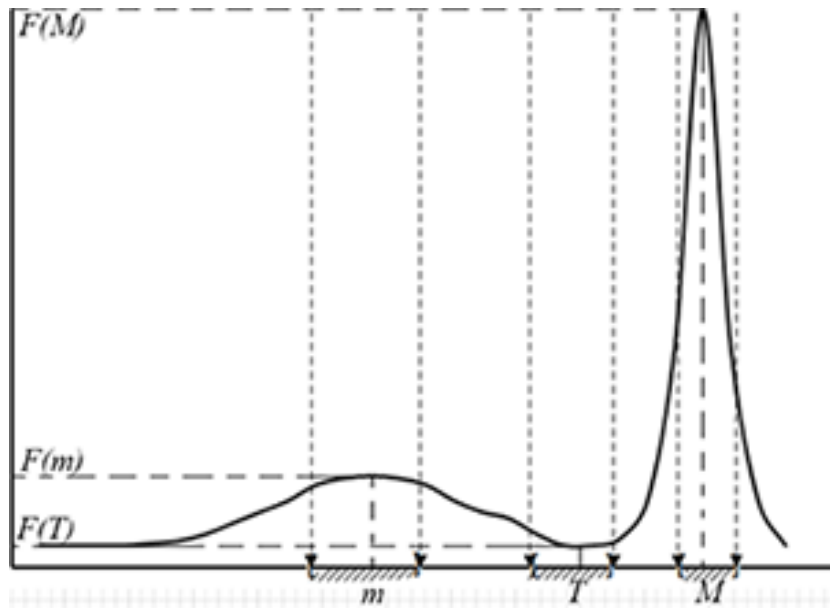


Fig. 7. Diagram of parameters of the image histograms

Having applied the Otsu method and found the brightness threshold value, we may find positions of discrete function maximum for each part of the histogram. A block diagram for classifying images of a low contrast ratio on the basis of the brightness histogram is given in Fig. 8. The search is conducted by a simple enumeration of discrete function values of the histogram in each part.

The block diagram given in Fig. 8 includes blocks:

- block 1 reads full-color images of continuous cast billet sulfur prints from a medium and loads into memory as a numeric array, every element of such array corresponds to a pixel color value;
- block 2 builds the brightness histogram for all three channels (red, green, blue) in the RGB color space;
- converts full-color images into gray-scale ones applying the algorithm BT709;
- block 4 builds the histogram of the image generated at a previous stage;
- blocks 5 and 6 search values which characterize shape-generating parameters of a histogram;
- block 7 creates a database containing data on results: an original image, a gray-scale image, discrete functions to build histograms for red, green, and blue channels, as well as the gray-scale image, brightness threshold and the value of the histogram in this point, maximum positions in both parts of the histogram and their values. A detailed diagram of functioning of blocks 5 and 6 is given in Fig. 9.

On the basis of shape-generating properties of the brightness histogram for images made in the first series of the experiment we got the results given in Table 1. Table 1 introduces notations:  $T_r, T_g, T_b, T_{gs}$  – discrete function values for the brightness threshold

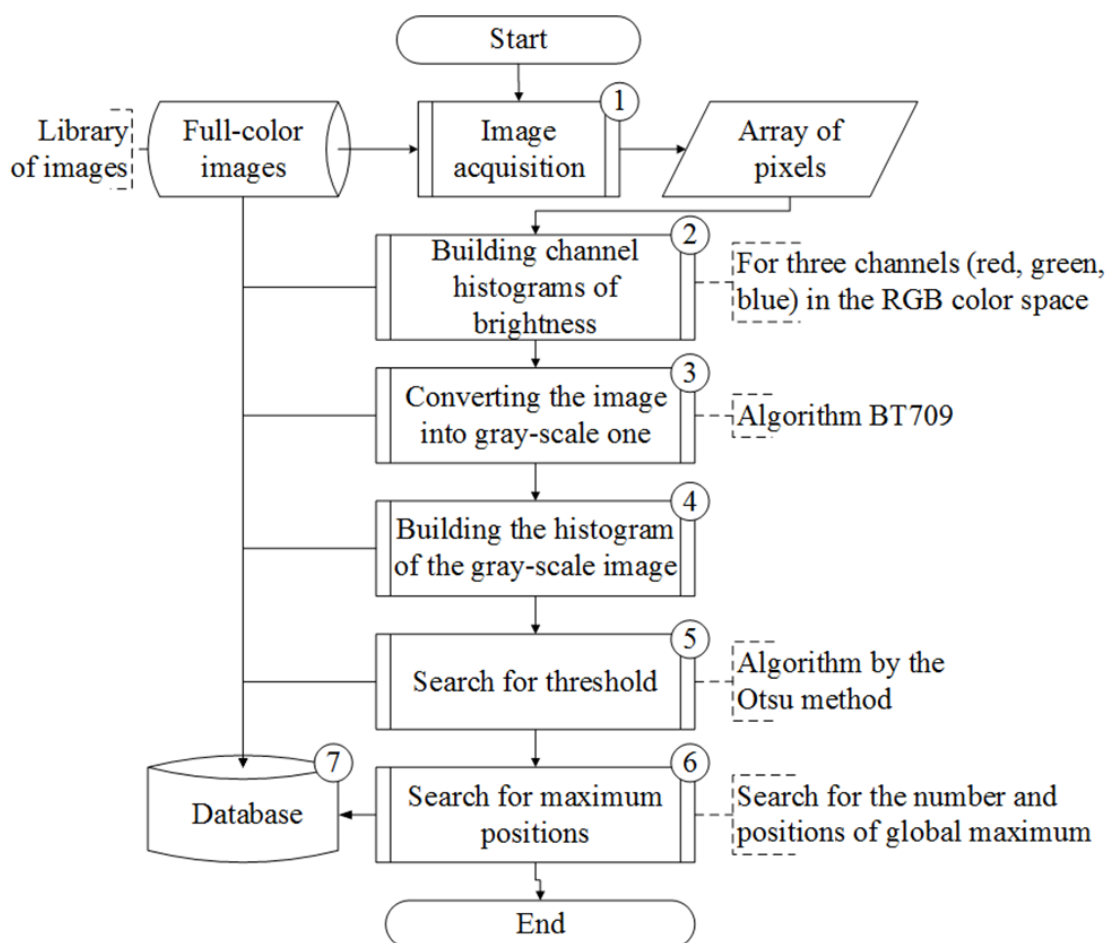


Fig. 8. A block diagram for classifying images on the basis of the brightness histogram

of every channel and gray-scale image;  $m_r, m_g, m_b, m_{gs}$  – maximum to the left of the brightness threshold of the discrete function of the histogram for every channel and gray-scale image;  $M_r, M_g, M_b, M_{gs}$  – maximum to the right of the brightness threshold of the discrete function of the histogram for every channel and gray-scale image;  $r, g, b$  – indices to denote color channels: red, green, blue correspondingly;  $gs$  – index of correspondence with the gray-scale image.

Table 1

Evaluation of the brightness threshold and maximum values of the discrete function for test images

Images	Red channel			Green channel			Blue channel			Gray scale		
	$m_r$	$T_r$	$M_r$	$m_g$	$T_g$	$M_g$	$m_b$	$T_b$	$M_b$	$m_{gs}$	$T_{gs}$	$M_{gs}$
Fig. 3a	241	242	245	237	238	245	227	228	245	237	238	240
Fig. 3b	189	214	255	178	205	255	151	190	255	179	206	254
Fig. 3c	169	204	249	151	198	249	151	181	235	152	197	248

In view of the values stated in Table 1, we divided images into groups and drew up classification Table 2.

Table 2

Classification of gray-scale images of sulfur prints of continuous cast billet transverse templates

Group	Number of images	Indicators					
		Left maximum		Brightness threshold		Right maximum	
		min	max	min	max	min	max
A	4	234	239	237	240	240	244
B	21	179	218	206	231	233	254
C	7	147	185	193	207	238	248

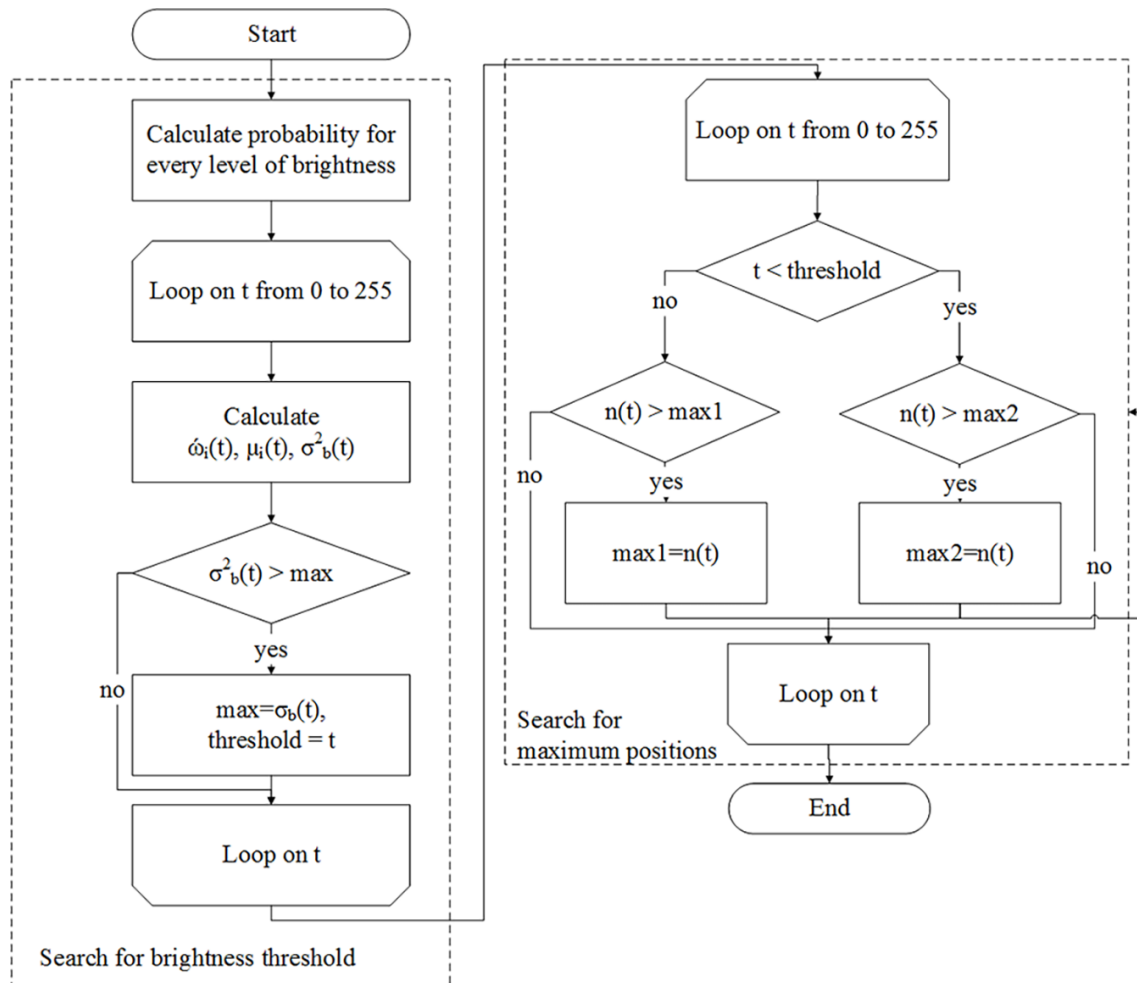


Fig. 9. A block diagram for searching for the brightness threshold value and maximum of the discrete function of the image histogram

Results given in Table 2 allow for using a technique for classification of images by shape-generating parameters of the brightness histogram with the adaptive membership function:

$$R = \sum_{i=0}^3 i \cdot [(m_{i \min} \leq m \leq m_{i \max}) \wedge (T_{i \min} \leq T \leq T_{i \max}) \wedge (M_{i \min} \leq M \leq M_{i \max})],$$

where  $R$  – a set of possible decisions consisting of four elements  $\{0, 1, 2, 3\}$ , whose value refers to image groups: 1 – group A; 2 – group B; 3 – group C; 0 – group consisting of images not included in any groups of classification;  $m_{i\ min}, m_{i\ max}, T_{i\ min}, T_{i\ max}, M_{i\ min}, M_{i\ max}$  – empirical limits of the threshold, left maximum and right maximum determined on the basis of an empirical study and adapted during training the decision-making system for classification of images;  $m, T, M$  – quantitative characteristics of the histogram of the image selected for classification: left maximum, threshold, and right maximum, correspondingly.

A block diagram for classifying images on the basis of the adaptive membership function is given in Fig. 10.

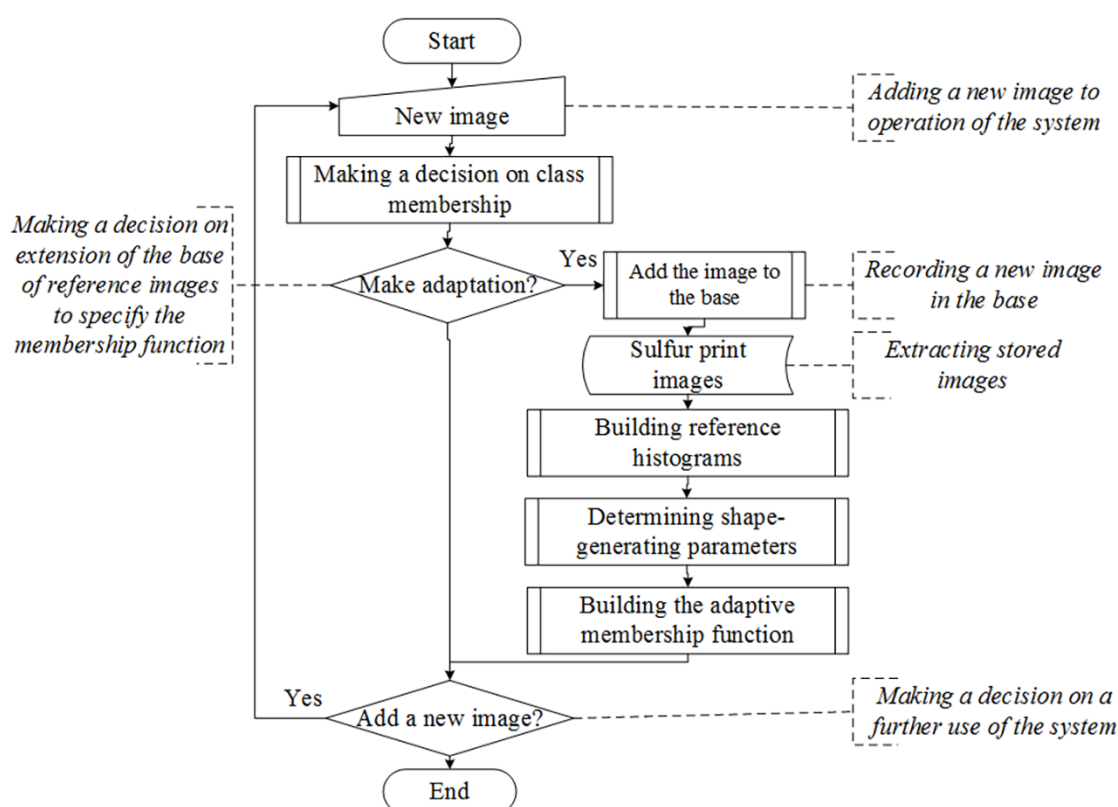


**Fig. 10.** A block diagram to make a decision on classification of images by shape-generating parameters of the sulfur print image brightness histogram on the basis of the adaptive membership function

On the basis of shape-generating parameters the number of images which were classified in an area of ambiguous identification amounted to: 31% – between classes A and B; 18% – between classes A and C; 78% – between classes B and C. Therefore, it was resolved to specify the developed classification technique.

### 1.3. A Technique to Classify Sulfur Print Images on the Basis of a Distance to a Reference Histogram

By dividing all sets of histograms into uniform classes, we may choose a path of image processing depending on its features.

To specify membership of images included in the area of ambiguous identification, one of classes was reviewed in terms of the distance between levels of the reference histogram of the class and levels of histograms of every of original images for every class. The number of compared parameters increases from 3 originally selected ones to 256. At the first stage the task was to determine a criterion of unambiguous classification of images as part of the proposed technique. Three types of distances were considered: the Euclidean distance, the Chebyshev distance, and the Manhattan distance:

- the Euclidean distance:

$$d_{kl} = \sqrt{\frac{1}{m} \sum_{j=1}^m (Z_{kj} - Z_{lj})^2}, \quad k, l = 1, \dots, n;$$

- the Chebyshev distance:

$$d_{kl} = \max |Z_{kj} - Z_{lj}|;$$

- the Manhattan distance:

$$d_{kl} = \frac{1}{m} \sum_{j=1}^m |Z_{kj} - Z_{lj}|,$$

where  $m$  – number of indicators  $X$ ;  $Z_{kj}$ ,  $Z_{lj}$  – standardized values of the indicator  $j$  for the  $k$ -th and  $l$ -th objects correspondingly;  $n$  – number of images.

Diagrams of scattering of distances from the normed reference histogram of every image are given in Fig. 11.

An image may be deemed to be classified unambiguously, if a value of every type of distance between the image histogram and histogram of a specific class is minimum. Fig. 12 presents a block diagram for classifying images. The block diagram of the algorithm includes:

- block 1 – reading full-color images of sulfur prints of continuous cast billet from a medium and loading into memory as an array of pixels;
- block 2 – converting full-color images into gray-scale ones applying the algorithm BT709;
- block 3 – building the histogram of the image generated at a previous stage;
- block 4 – calculating three types of distances between the current image histogram and reference histograms of classes;
- block 5 – searching for the class with minimum distances of all types.

#### 1.4. A Technique to Eliminate Ambiguous Identification of Images on the Basis of a Fuzzy Set

As after applying techniques based on shape-generating parameters of histograms and distances 31% of images are left in the area of ambiguous identification, the technique for classifying sulfur prints on the basis of a fuzzy set was developed.

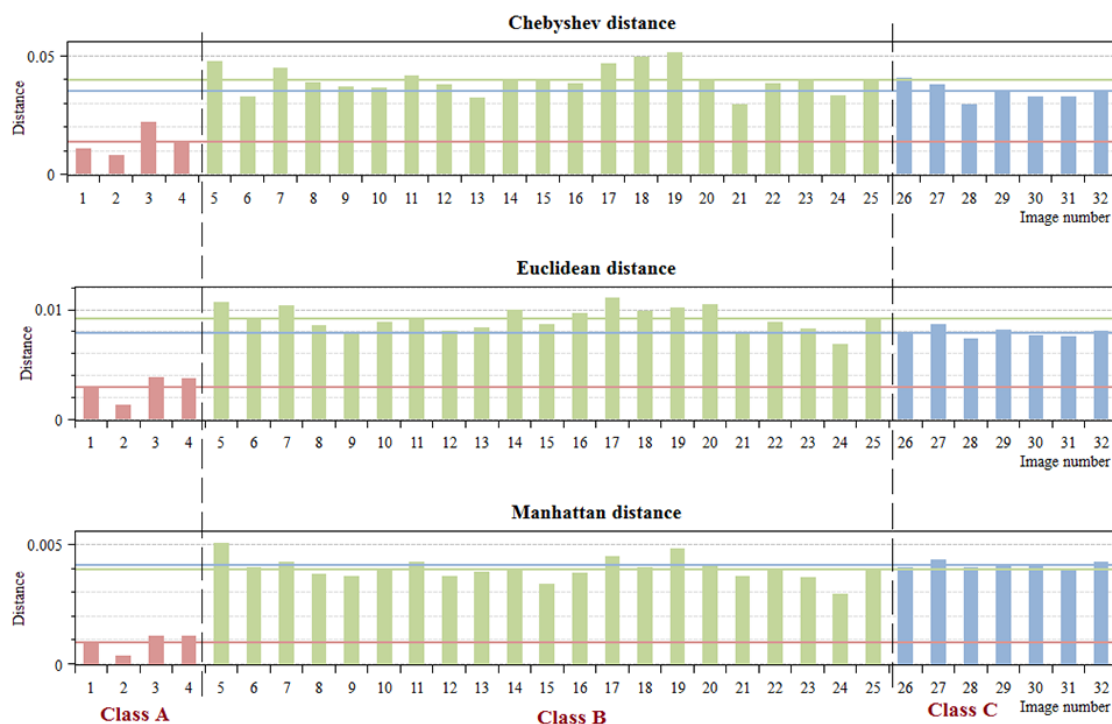


Fig. 11. Diagrams of scattering of distances from every diagram to reference ones for class B

The most complicated stage in applying fuzzy sets to solve applied problems is determination of linguistic variables and their terms. To solve the task of classification of images, we introduce a structured linguistic variable – *Image*, which contains six components:  $m$ ,  $M$ ,  $T$ ,  $d_A$ ,  $d_B$ ,  $d_C$ , where  $T$  – position of a brightness threshold;  $m$  – position of brightness left maximum;  $M$  – position of brightness right maximum;  $d_A$ ,  $d_B$ ,  $d_C$  – the Chebyshev distance to reference histograms  $A$ ,  $B$  and  $C$  correspondingly. Fig. 13 gives the structure of the linguistic variable – *Image*.

Every component of the linguistic variable *Image* takes three values: "Member of class A", "Member of class B", "Member of class C".

Every component of the key linguistic variable is set to a basic numeric variable and a membership function. Fig. 14 and 15 give the structure of two linguistic components corresponding to the basic numeric variable and the membership function built on the basis of expert information. Distribution of values of the basic variable corresponds to results given in Table 2. Fig. 14 introduces notations:  $m_B$  – basic numeric variable corresponding to linguistic one  $m$ ;  $m_{A\ min}$ ,  $m_{B\ min}$ ,  $m_{C\ min}$  – lower limit of the basic variable  $m_B$ ;  $m_{A\ max}$ ,  $m_{B\ max}$ ,  $m_{C\ max}$  – upper limit of the basic variable  $m_B$ ;  $\mu_m$  – membership function for the component  $m$ . Upper and lower limits may vary, when the system is adapted due to input of new sulfur print images in the database.

Fig. 15 introduces notations:  $M_B$  – basic numeric variable corresponding to linguistic one  $M$ ;  $M_{A\ min}$ ,  $M_{B\ min}$ ,  $M_{C\ min}$  – lower limit of the basic variable  $M_B$ ;  $M_{A\ max}$ ,  $M_{B\ max}$ ,  $M_{C\ max}$  – upper limit of the basic variable  $M_B$ ;  $\mu_M$  – membership function for the component  $M$ .

Every component and key linguistic variable are defuzzified by one of known methods. For example, by the highest membership degree or by the method of the center of gravity.

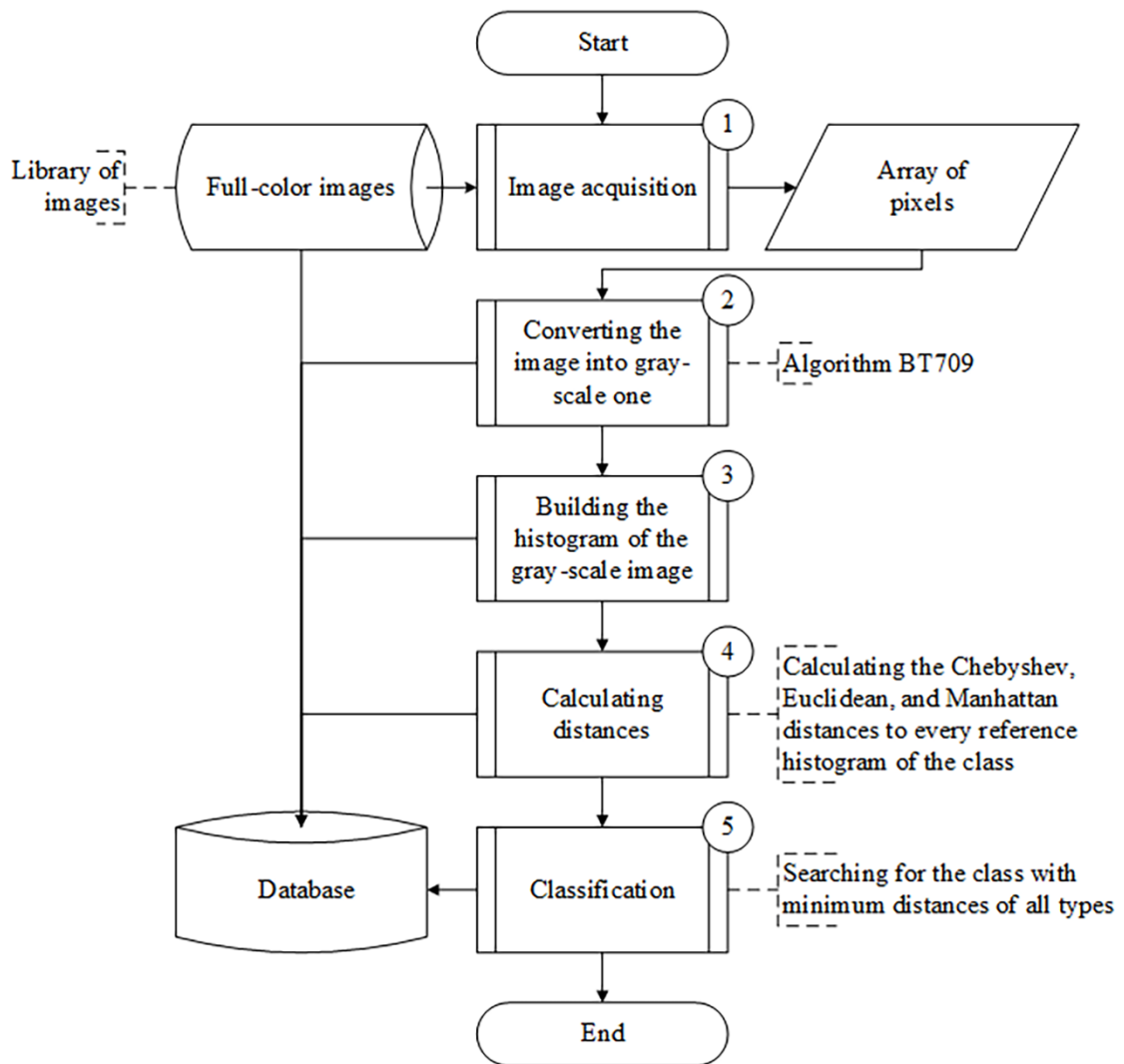


Fig. 12. A block diagram for classifying images

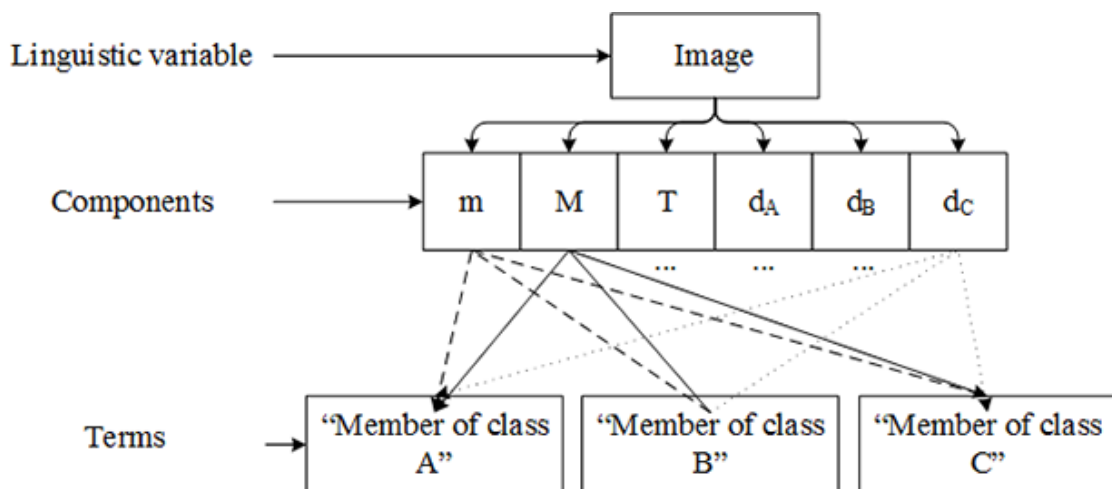


Fig. 13. A structure of the linguistic variable image

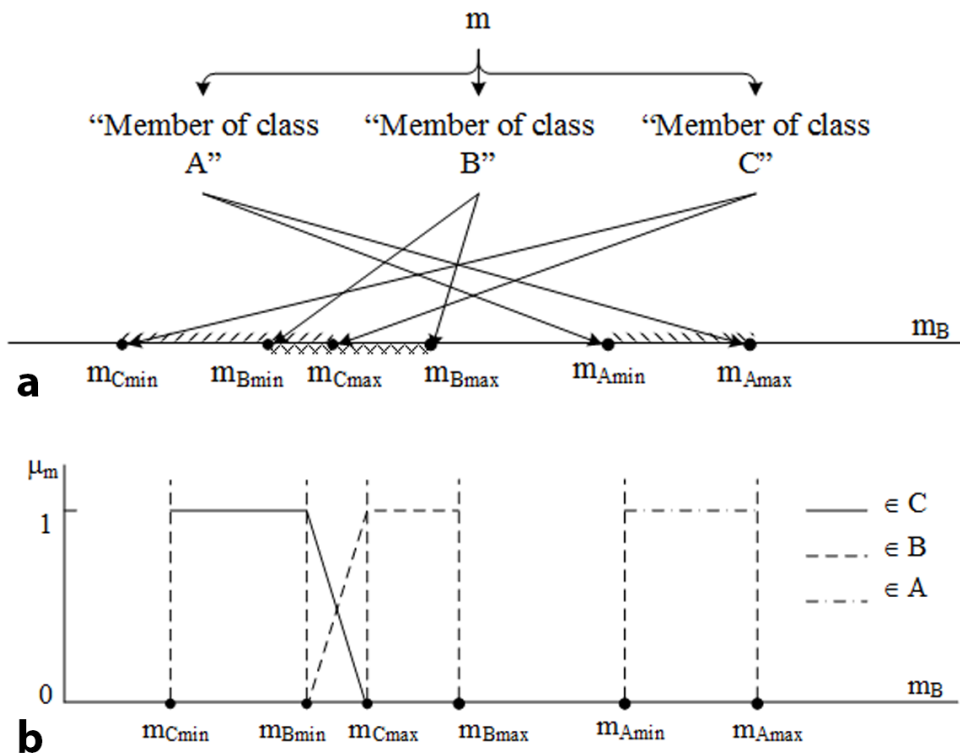


Fig. 14. Linguistic component  $m$ : a – structure of the variable; b – membership function

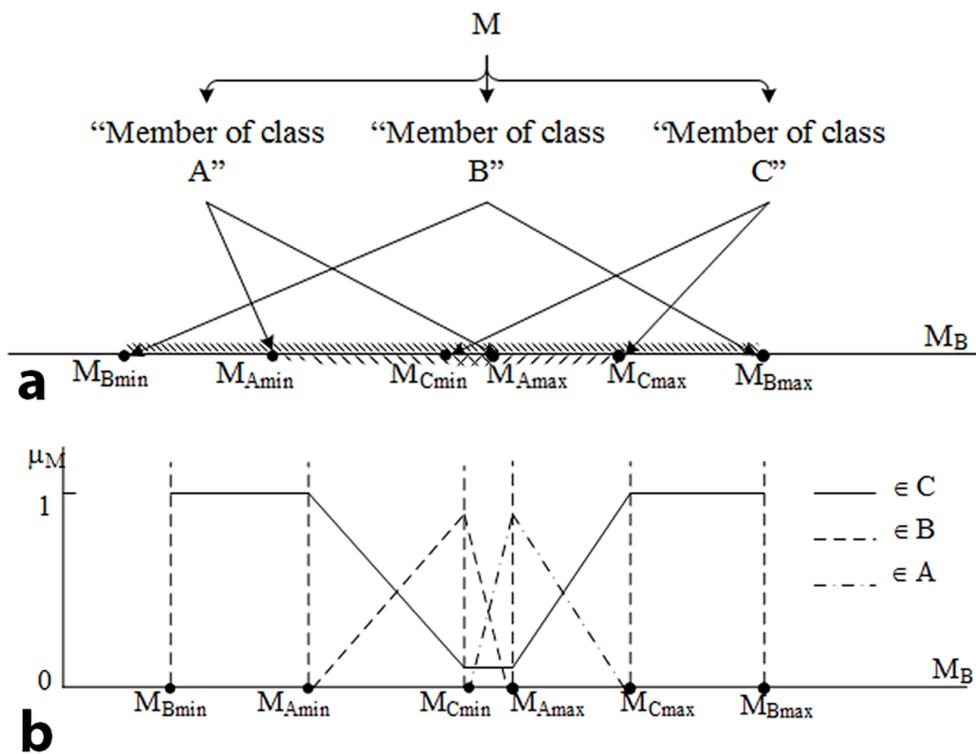


Fig. 15. Linguistic component  $M$ : a – structure of the variable; b – membership function

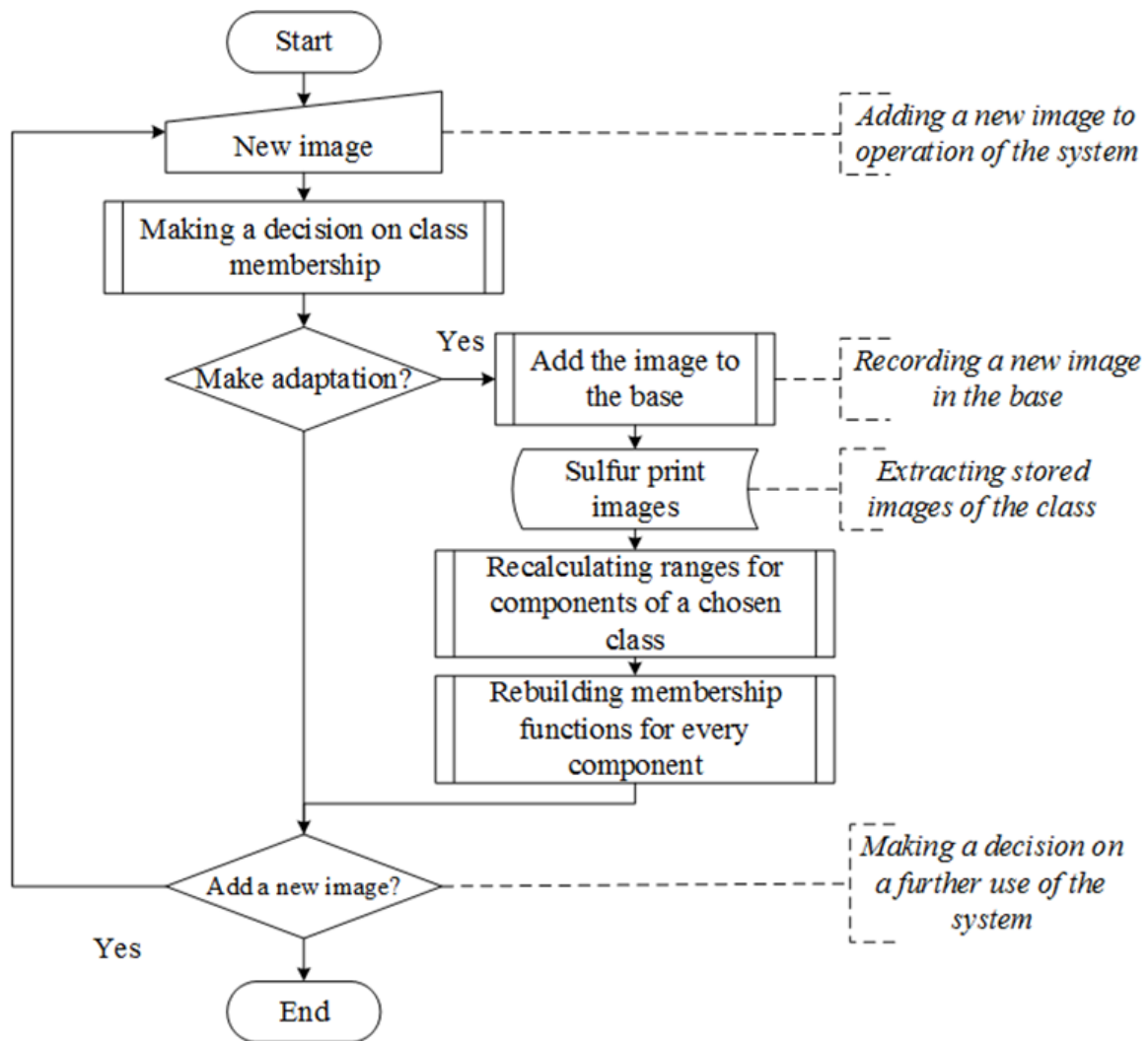


Fig. 16. A block diagram for classification on the basis of a theory of fuzzy logic

A block diagram for classifying images on the basis of fuzzy sets is given in Fig. 16. The algorithm includes blocks of defuzzification for every linguistic component and the key linguistic variable Image by the highest membership degree.

As this technique does not allow for areas of ambiguous identification, all images under review will be attributed to one of three introduced classes and every class will have a definite path of further specification of a line of the object under study and its filling with objects of a non-regular form corresponding to defects in the metal continuity.

### 1.5. An Adaptive Technique of Cascade Classification of Graphical Data on the Quality of Continuous Cast Billets

Studying a structure of the original image and techniques for its classification on the principle of from simple to complex resulted in development of a cascade technique for classifying sulfur prints. Every next cascade of classification is applied to images located in an area of ambiguous identification on the basis of an evaluation of a previous step. Every formed cascade differs from a previous one in a number of identification indicators

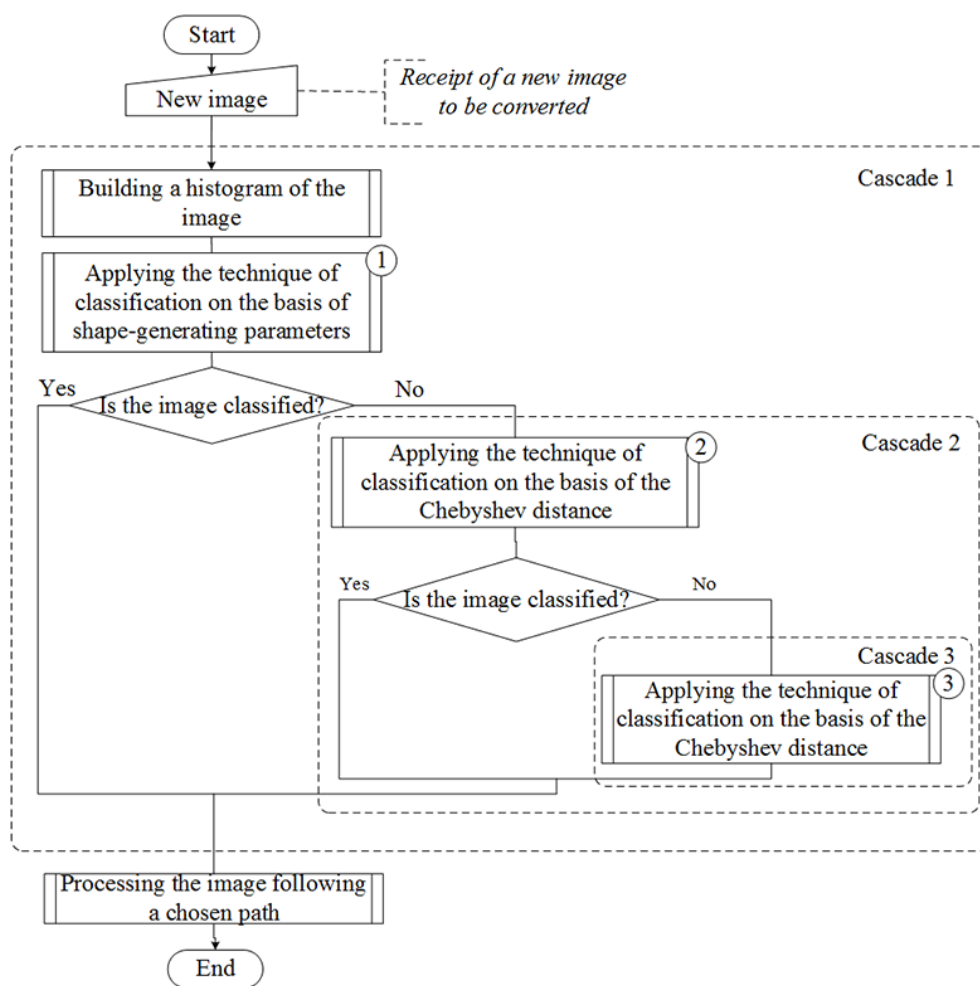


**Fig. 17.** A block diagram of the adaptive technique of cascade classification of continuous cast billet transverse template sulfur print images

and complexity of membership functions. Fig. 17 gives a block diagram of the adaptive technique of cascade classification of sulfur print images. All blocks 1-3 of the cascade classification technique contain adaptive blocks according to block diagrams given in Fig. 10, 12 and 16.

Attribution of the image to a selected class allowed for determination of a path to process information about the quality of continuous cast billets under OST 14-1-236-91.

## 2. Results of Cascade Classification of Sulfur Print Images of Billet Transverse Templates

The above techniques are implemented in software Cascade – Sulfur Print

### 2.1. Results of Image Classification on the Basis of Shape-Generating Parameters of Histograms

Every class of images had histograms having specific differences in the form:

1. Histograms of images of class A are unimodal, as the background and the object under study have comparatively similar brightness. Significant levels of brightness are located in a narrow (10 ÷ 15% within a range of [215; 255]) band characterizing a low contrast of images. The band is shifted to the left evidencing of high brightness of images.
2. Histograms of images of class B are characterized by two expressed peaks comparable in terms of an area as the background and the object under study have different brightness. Significant levels of brightness are located in a band with the width of 40 ÷ 50% within a range of [140; 255] – the image has a normal contrast.
3. Histograms of images of class C also have two peaks, however, the left one is located in a wider band and has lower maximum. The background and the object under study significantly differ in brightness.

The width of the band of significant levels of brightness is 70% within a range of [80; 255], corresponding to a high-contrast image. The obtained histograms of every class showed that:

1. The histogram of a grayscale image is enough to classify images, as deviation of the threshold and maximum values of channel histograms compared to the histogram of grayscale images does not exceed 15%.
2. An original assumption on a division of the set of images into three classes is confirmed with results of the computational experiment, and there is a need for development of a technique for identifying a form of sulfur print image histogram.

We built average normed histograms for every class of images. Such histograms were adopted as reference ones, Figure 18 gives reference histograms for all classes.

The form of the above histograms allows for putting forward a hypothesis on possible classification of images by the form of the histogram. Having analyzed histograms, we proposed an adaptive function of mapping of every image to one of three classes:

$$R = \sum_{i=0}^3 i \cdot [(m_{i \min} \leq m \leq m_{i \max}) \wedge (T_{i \min} \leq T \leq T_{i \max}) \wedge (M_{i \min} \leq M \leq M_{i \max})],$$

where  $R$  – set of possible decisions consisting of four elements  $\{0, 1, 2, 3\}$ , whose values correspond to groups of images: 1 – group A; 2 – group B; 3 – group C; 0 – group consisting of images not included in any groups of classification;  $m_{i \min}$ ,  $m_{i \max}$ ,  $T_{i \min}$ ,  $T_{i \max}$ , – empirical limits of the threshold, left maximum and right maximum determined on the basis of an empirical study and adapted during training the decision-making system for classification of images;  $m$ ,  $T$ ,  $M$  – quantitative characteristics of the histogram of the image selected for classification: left maximum, threshold, and right maximum, correspondingly.

Having analyzed diagrams, we made an assumption that there are areas of ambiguous identification. Having sorted out empirical parameters in ascending order and analyzed their location along the axis of brightness of points of images, we confirmed our assumption for initial empirical material.

An analytical rule of class membership was established for all classes:

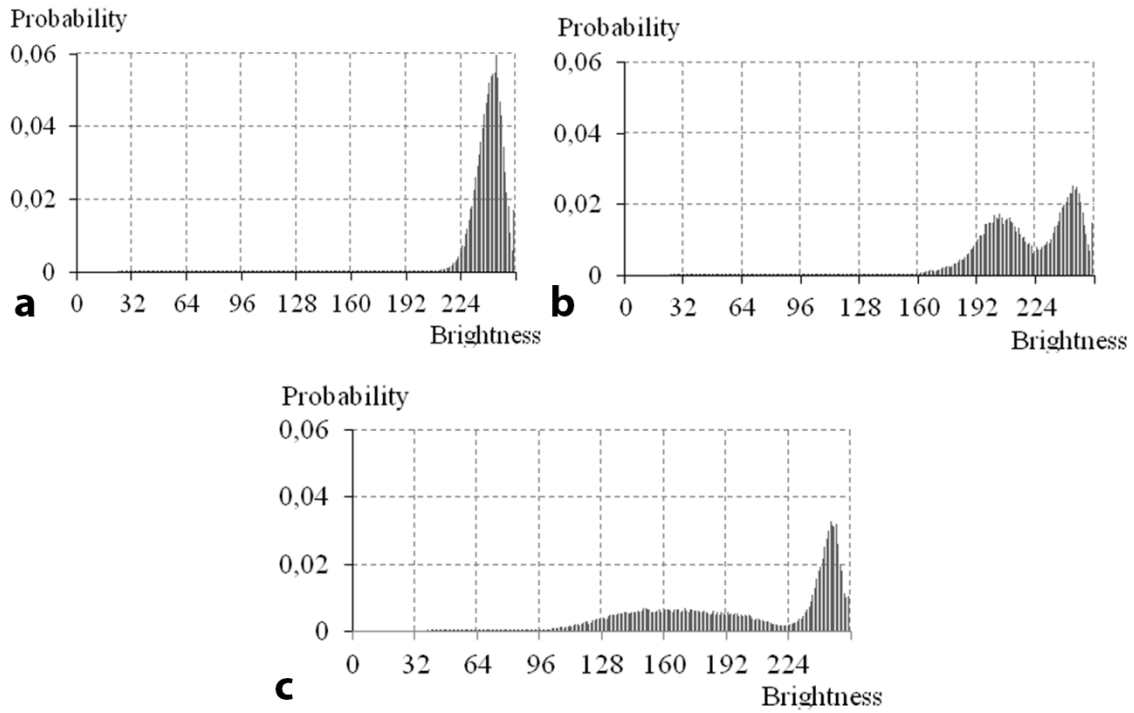


**Fig. 18.** Average normalized histograms for classes of images: a – for images of class A; b – for images of class B; c – for images of class C

1.  $\forall M (M \in [M_{min A}; M_{max A}]) \Rightarrow (A \subset B)$ , i.e. for any tuple  $(m, T, M)$ , where  $M \in [M_{min A}; M_{max A}]$  histograms are identified by two values from the set  $R$  (see Fig. 18a).
2.  $\forall M (M \in [M_{min C}; M_{max A}]) \Rightarrow (A \subset C)$ , i.e. for any tuple  $(m, T, M)$ , where  $M \in [M_{min C}; M_{max A}]$  histograms are identified by two values from the set  $R$  (see Fig. 18b).
3.  $\forall m (m \in [m_{min B}; m_{max C}]) \ \& \ \forall T (T \in [T_{min B}; T_{max C}]) \ \& \ M (M \in [M_{min C}; M_{max C}]) \Rightarrow (B \subset C)$ , i.e. for any tuple  $(m, T, M)$ , where  $m \in [m_{min B}; m_{max A}]$ ,  $T \in [T_{min B}; T_{max C}]$  and  $M$  is a relevant component of histograms from class C, histograms are identified by two values from the set  $R$  (see Fig. 18c).

Having represented the areas of ambiguous identification as logical expressions, we obtain:

$$(M_{min A} < M < M_{max A}) \rightarrow (A \subset B) \Rightarrow \overline{(M_{min A} < M < M_{max A})} \vee (A \subset B); \quad (1)$$

$$(M_{min C} < M < M_{max A}) \rightarrow (A \subset C) \Rightarrow \overline{(M_{min C} < M < M_{max A})} \vee (A \subset C); \quad (2)$$

$$\begin{aligned} (m_{min B} < m < m_{max C}) \wedge (T_{min C} < T < T_{max C}) \wedge (M_{min C} < M < M_{max C}) \rightarrow \\ \rightarrow (B \subset C) \Rightarrow \overline{(m_{min B} < m < m_{max C})} \vee \overline{(T_{min C} < T < T_{max C})} \vee \\ \vee \overline{(M_{min C} < M < M_{max C})} \vee (B \subset C). \end{aligned} \quad (3)$$

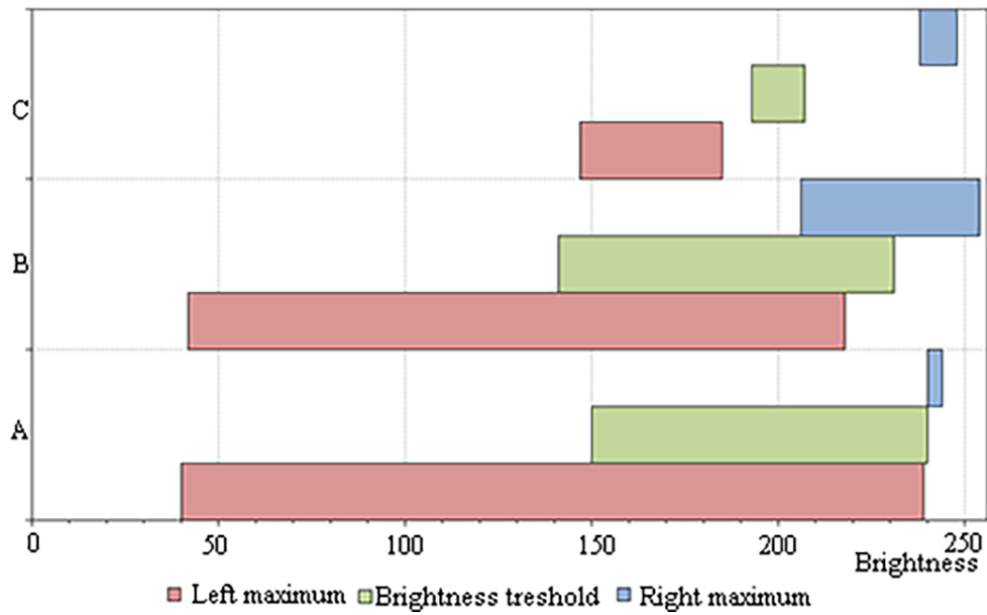


Fig. 19. Areas of ambiguous identification of mapping  $X(R)$

Then a total area of ambiguous identification (see Fig. 19) may be written as:

$$X(R) = (1) \vee (2) \vee (3) \Rightarrow (m_{\min B} < m < m_{\max C}) \wedge (T_{\min C} < T < T_{\max C}) \wedge (M_{\min A} < M < M_{\max C}) \rightarrow (M_{\min A} < M < M_{\max C}) \rightarrow \rightarrow ((A \subset B) \vee (A \subset C) \vee (B \subset C)).$$

Conclusions:

1. When the technique for classifying images on the basis of shape-generating parameters of histograms is applied, areas of ambiguous identification appear.
2. The size of areas of ambiguous identification is as follows:  $m_B \cap m_C = [179, 185]$ ,  $T_B \cap T_C = [206, 207]$ ,  $M_A \cap M_B = [240, 244]$ ,  $M_A \cap M_C = [240, 244]$ ,  $M_B \cap M_C = [238, 248]$ .
3. The number of images which were in the area of ambiguous identification during classification was 31% – between classes A and B; 18% – between classes A and C; 78% – between classes B and C.
4. Classification indicators may be specified, if the number of points of comparison with the reference histogram increases.

Only 22% of original images were unambiguously classified on the basis of shape-generating histograms.

## 2.2. Results of Classification of Images on the Basis of Distances

Regarding 78% of ambiguously identified images, we calculated three types of distances (see p. 1.3) and evaluated membership of every class. The membership rule was as follows:

an image is attributed to a set class, if all three types of distances have a minimum value. If we introduce notations  $S_{ij}$  – distance with the number  $i$  to a class with the number  $j$ , the matrix will be as follows:

		Class, $j$		
		A	B	C
Distance type, $i$		1	2	3
	Chebyshev,	1	$S_{11}$	$S_{12}$
Euclidean,	2	$S_{21}$	$S_{22}$	$S_{23}$
Manhattan,	3	$S_{31}$	$S_{32}$	$S_{33}$

In view of the introduced notations, the analytical expression of the class condition is:  $\forall i = \overline{1, 3} \exists j = \text{const} (S_{i \min} = d_{ij}) \rightarrow I \in K_j$ , where  $S_{i \min}$  – minimum distance of  $i = \overline{1, 3}$ ;  $I$  – formal notation of the image;  $K_j$  – notation of the class with the number  $j = \overline{1, 3}$ .

Figure 20 gives diagrams with calculated distances of every type for unambiguous classified images. For every series of images, the matrix of distances is as follows:

– for figure 20a

	A	B	C
1	0.0320	0.0120	0.0230
2	0.0100	0.0022	0.0060
3	0.0038	0.0012	0.0037

– for figure 20b

	A	B	C
1	0.0104	0.017	0.0095
2	0.0028	0.010	0.0085
3	0.0008	0.0041	0.0048

For Fig. 20a all minimum distances correspond to class B, therefore, images are classified unambiguously. For Fig. 20b classification for classes A and C is ambiguous. In this case it is necessary to perform the third cascade step. At the second cascade step 70% of the rest images were identified unambiguously.

At the third cascade step all the rest images were classified unambiguously. Results of classification are given in Table 3.

### 3. Conclusions

1. The experimental survey resulted in preparation of a base of sulfur print images and on the basis of their visual examination main structural parts were determined: "the object under study" and "background". Regarding brightness of the determined parts, it was proposed to divide all images into three classes: A, B and C. By attributing images to one of specified classes, a path of further image processing is determined.

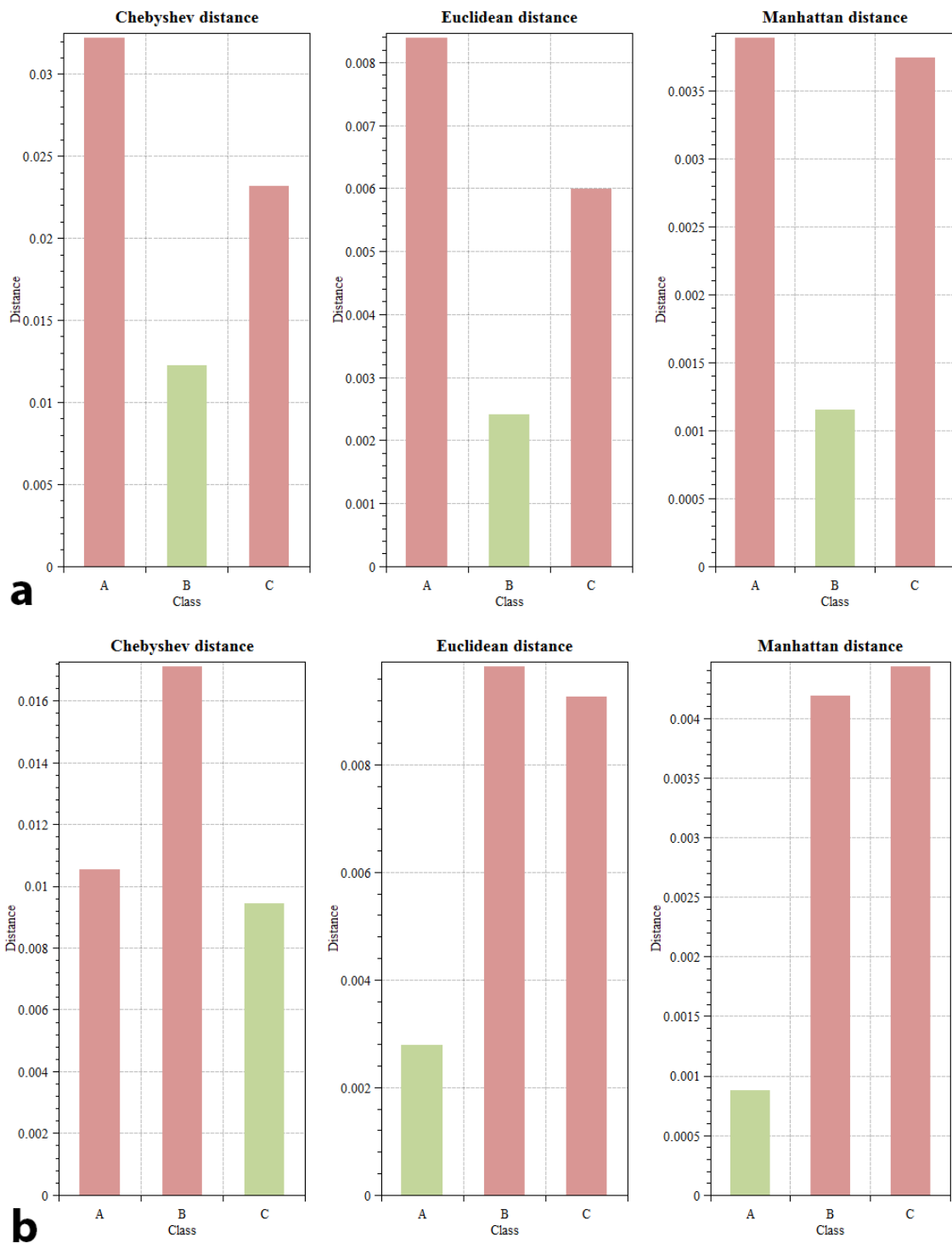


**Fig. 20.** Diagrams with calculated distances of all types: a – for the unambiguously classified image; b – for the ambiguously classified image

**Table 3**

Classification of images when the technique of cascade classification is applied

No.	Image name in the project	Results of classification			
		visual	shape-generating parameters	distances	fuzzy sets
1	29.tiff	A	A, B, C	C, A	A
2	30.tiff	A	A, B, C	C, A	A
3	31.tiff	A	A, B, C	C, A	A
4	32.tiff	A	A, B, C	C, A	A
5	01.tiff	B	B, C	B	B
6	02.tiff	B	A, B, C	C, B	B
7	03.tiff	B	B	B	B
8	04.tiff	B	B, C	C, B	B
9	05.tiff	B	A, B, C	C, B	B
10	06.tiff	B	A, B, C	C, B	B
11	07.tiff	B	B	B	B
12	08.tiff	B	B, C	B	B
13	09.tiff	B	B, C	B	B
14	10.tiff	B	B, C	C, B	B
15	11.tiff	B	B, C	B	B
16	12.tiff	B	B, C	C, B	B
17	13.tiff	B	B	B	B
18	14.tiff	B	B, C	B	B
19	15.tiff	B	B, C	B	B
20	16.tiff	B	A, B, C	B	B
21	17.tiff	B	A, B, C	B	B
22	18.tiff	B	A, B, C	B	B
23	19.tiff	B	B, C	B	B
24	20.tiff	B	A, B, C	B	B
25	21.tiff	B	B, C	B	B
26	22.tiff	C	B, C	C	C
27	23.tiff	C	B, C	C	C
28	24.tiff	C	B, C	C	C
29	25.tiff	C	B, C	C	C
30	26.tiff	C	A, B, C	C	C
31	27.tiff	C	A, B, C	C	C

2. A brightness histogram was chosen as a key characteristic of the sulfur print image. A normed reference histogram was built for every supposed class; the shape of such histogram may be characterized by three key shape-generating parameters and 256 levels of brightness.
3. A technique was developed to classify sulfur print images on the basis of the membership function by three shape-generating parameters of the histogram. As a result, 22% of images were attributed to the area of unambiguous classification.

4. Regarding images attributed to the area of ambiguous identification, a technique was developed on the basis of calculation of the Chebyshev distance for 256 levels of the histogram. Upon application of this technique, 70% of the other images were classified.
5. To eliminate areas of ambiguous identification, it was proposed to apply the technique based on the theory of fuzzy sets for a complex structured linguistic variable "Image" consisting of six components. Term sets and membership functions were introduced for every component as recommended by experts. At the third cascade step all images were classified unambiguously.

## References

1. Logunova O.S., Matsko I.I., Posokhov I.A., Luk'ynov S.I. Automatic System for Intelligent Support of Continuous Cast Billet Production Control Processes. *The International Journal of Advanced Manufacturing Technology*, 2014, vol. 74, no. 9, pp. 1407–1418. doi: 10.1007/s00170-014-6056-4
2. Matsko I.I., Snegirev Y.V., Logunova O.S. Data Acquisition and Preparation Methods for Continuously Cast Billets Quality Analysis Software. *Applied Mechanics and Materials*, 2012, vol. 110-116, pp. 3557–3562. doi: 10.4028/www.scientific.net/AMM.110-116.3557
3. Logunova O.S. Internal-Defect Formation and the Thermal State of Continuous-Cast Billet. *Steel in Translation*, 2008, vol. 38, no. 10, pp. 849–852. doi: 10.3103/S0967091208100148
4. Chapelle O., Haffner P., Vapnik V. Support Vector Machines for Histogram-Based Image Classification. *IEEE Transactions on Neural Networks*, 1999, vol. 10, no. 5, pp. 1055–1064. doi: 10.1109/72.788646
5. Foody G.M., Mathur A. A Relative Evaluation of Multiclass Image Classification by Support Vector Machines. *IEEE Transactions on Geoscience and Remote Sensing*, 2004, vol. 42, no. 6, pp. 1335–1343. doi: 10.1109/TGRS.2004.827257
6. Lyons M., Budynek J., Akamatsu S. Automatic Classification of Single Facial Images. *IEEE Transactions on Pattern Analysis and Machine Intelligence*, 1999, vol. 21, no. 12, pp. 1357–1362. doi: 10.1109/34.817413
7. Leemput K.V., Maes F., Vandermeulen D., Suetens P. Automated Model-Based Tissue Classification of MR Images of the Brain. *IEEE Transactions on Medical Imaging*, 1999, vol. 18, no. 10, pp. 897–908. doi: 10.1109/42.811270
8. Varma M., Zisserman A. A Statistical Approach to Texture Classification from Single Images. *International Journal of Computer Vision*, 2005, vol. 62, no. 1-2, pp. 61–81.
9. Wang F. Fuzzy Supervised Classification of Remote Sensing Images. *IEEE Transactions on Geoscience and Remote Sensing*, 1990, vol. 28, no. 2, pp. 194–201.
10. Wang F., Newkirk R. Design and Implementation of Knowledge-Base System for Remotely Sensed Change Detection. *Journal of Imaging Techn.*, 1987, vol. 13, pp. 116–122.
11. Cannon R.L., Dave J.V., Bezdek J.C., Kolsky H.G. Segmentation of a Thematic Mapper Image Using the Fuzzy C-Means Clustering Algorithm. *IEEE Transactions on Geoscience and Remote Sensing*, 1986, vol. GE-24, no. 3, pp. 400–408.

12. Morlini I., Zani S. A New Class of Weighted Similarity Indices Using Polytomous Variables. *Journal of Classification*, 2012, vol. 29, no. 2, pp. 199–226. doi: 10.1007/s00357-012-9107-2
13. Giordani P., Kiers H. FINDCLUS: Fuzzy Individual Differences CLUstering. *Journal of Classification*, 2012, vol. 29, no. 2, pp. 170–198. doi: 10.1007/s00357-012-9109-0
14. Contreras P., Murtagh F. Fast, Linear Time Hierarchical Clustering Using the Baire Metric. *Journal of Classification*, 2012, vol. 29, no. 2, pp. 118–143. doi: 10.1007/s00357-012-9106-3
15. Bar-Hen A., Gey S., Poggi J.M. Influence Measures for CART Classification Trees. *Journal of Classification*, 2015, vol. 32, no. 1, pp. 21–45. doi: 10.1007/s00357-015-9172-4
16. Shestakov A.L., Sviridyuk G.A. On a New Concept of White Noise. *Review of Applied and Industrial Mathematics*, 2012, vol. 19, no. 2, pp. 287–288. (in Russian)
17. Shestakov A.L., Sviridyuk G.A., Khudyakov Y.V. Dynamic Measurement in Spaces of „noise“. *Bulletin of the South Ural State University. Series: Computer Technologies, Automatic Control and Radioelectronics*, 2013, vol. 13, no. 2, pp. 4–11. (in Russian)
18. Poynton C. Rehabilitation of Gamma. *Proc. SPIE*, 1998, vol. 1998, pp. 232–242.
19. Stokes M., Anderson M., Chandrasekar S., Motta R. *A Standard Default Color Space for the Internet – sRGB*, available at: <http://www.w3.org/Graphics/Color/sRGB.html> (accessed on 6 December 2016).
20. Gonzalez R., Woods R. *Digital Image Processing*. Moscow, Tekhnosfera, 2005. (in Russian)
21. Shapiro L., Stockman J. *Computer vision*. Moscow, BINOM: Laboratory of knowledge, 2006. (in Russian)
22. Pratt W. *Digital Image Processing*, Moscow, Mir, 1982. (in Russian)
23. Otsu N.A. Threshold Selection Method from Gray-Level Histograms. *IEEE Transactions on Systems, Man and Cybernetics*, 1979, vol. 9, no. 1, pp. 62–66.
24. Ridler T.W., Calvard S. Picture Thresholding Using an Iterative Selection Method. *IEEE Trans. System, Man and Cybernetics*, 1978, vol. 8, no. 8, pp. 630–632.

*Ivan A. Posokhov, Department of Computer Engineering and Programming, Nosov Magnitogorsk State Technical University (Magnitogorsk, Chelyabinsk region, Russian Federation) posohoff@bk.ru.*

*Oxana S. Logunova, DSc (Techn), Professor, Department of Computer Engineering and Programming, Nosov Magnitogorsk State Technical University (Magnitogorsk, Chelyabinsk region, Russian Federation) logunova66@gmail.com.*

*Anatoly Yu. Mikov, Department of Computer Engineering and Programming, Nosov Magnitogorsk State Technical University (Magnitogorsk, Chelyabinsk region, Russian Federation) mikov.ayu@gmail.com.*

*Received November 29, 2016*

## МЕТОД И АЛГОРИТМЫ КАСКАДНОЙ КЛАССИФИКАЦИИ ИЗОБРАЖЕНИЙ СЕРНОГО ОТПЕЧАТКА ПОПЕРЕЧНОГО ТЕМПЛЕТА ЗАГОТОВКИ

*И.А. Посохов, О.С. Логунова, А.Ю. Миков*

В работе представлены результаты исследования изображений серных отпечатков поперечного темплетта непрерывнолитой заготовки. Авторами работы определены проблемы низкой достоверности информации о качестве заготовок. Визуальная оценка изображения приводит к субъективной оценке с большим вкладом человеческого фактора. Авторами разработана схема размещения точек контроля для сбора графической информации в процессе получения заготовок. Предложено ввести три класса изображений по признаку отношения яркости объекта (темплета) к основному фону. По нарастанию сложности алгоритмов авторами предложена каскадная методика классификации изображения. Методика включает оценку изображения по формообразующим характеристикам гистограммы, по расстоянию до эталонных нормированных гистограмм и на основе методов нечеткой логики. Результаты опытной эксплуатации каскадной методики получено: упрощенная методика по формообразующим характеристикам однозначно идентифицировала 22% всех изображений, по оценке расстояния до эталонных нормированных гистограмм – 70% от оставшихся и только оценка при применении методов нечеткой логики однозначно идентифицировала все оставшиеся изображения. Сто процентный успех классификации достигается только при применении всех каскадов разработанной методики.

*Ключевые слова: изображения серных отпечатков; гистограмма изображения; формообразующие характеристики; расстояния между объектами; правила идентификации объектов; каскадная классификация.*

### Литература

1. Logunova, O.S. Automatic System for Intelligent Support of Continuous Cast Billet Production Control Processes / O.S. Logunova, I.I. Matsko, I.A. Posokhov, S.I. Luk'ynov // The International Journal of Advanced Manufacturing Technology. – 2014. – V. 74, № 9. – P. 1407–1418. doi: 10.1007/s00170-014-6056-4
2. Matsko, I.I. Data Acquisition and Preparation Methods for Continuously Cast Billets Quality Analysis Software / I.I. Matsko, Y.V. Snegirev, O.S. Logunova // Applied Mechanics and Materials. – 2012. – V. 110-116. – P. 3557–3562. doi: 10.4028/www.scientific.net/AMM.110-116.3557
3. Logunova, O.S. Internal-Defect Formation and the Thermal State of Continuous-Cast Billet / O.S. Logunova // Steel in Translation. – 2008. – V. 38, № 10. – P. 849–852. doi: 10.3103/S0967091208100148
4. Chapelle, O. Support Vector Machines for Histogram-Based Image Classification / O. Chapelle, P. Haffner, V.N. Vapnik // IEEE Transactions on Neural Networks. – 1999. – V. 10, № 5. – P. 1055–1064. doi: 10.1109/72.788646
5. Foody, G.M. A Relative Evaluation of Multiclass Image Classification by Support Vector Machines / G.M. Foody, A. Mathur // IEEE Transactions on Geoscience and Remote Sensing. – 2004. – V. 42, № 6. – P. 1335–1343. doi: 10.1109/TGRS.2004.827257

6. Lyons, M. Automatic Classification of Single Facial Images / M. Lyons, J. Budynek, S. Akamatsu // IEEE Transactions on Pattern Analysis and Machine Intelligence. – 1999. – V. 21, № 12. – P. 1357–1362. doi: 10.1109/34.817413
7. Leemput, K.V. Automated Model-Based Tissue Classification of MR Images of the Brain / K.V. Leemput, F. Maes, D. Vandermeulen, P. Suetens // IEEE Transactions on Medical Imaging. – 1999. – V. 18, № 10. – P. 897–908. doi: 10.1109/42.811270
8. Varma, M. A Statistical Approach to Texture Classification from Single Images / M. Varma, A. Zisserman // International Journal of Computer Vision. – 2005. – V. 62, № 1-2. – P. 61–81.
9. Wang, F. Fuzzy Supervised Classification of Remote Sensing Images / F. Wang // IEEE Transactions on Geoscience and Remote Sensing. – 1990. – V. 28, № 2. – P. 194–201.
10. Wang, F. Design and Implementation of Knowledge-Base System for Remotely Sensed Change Detection / F. Wang, R. Newkirk // Journal Imaging Techn. – 1987. – V. 13. – P. 116–122.
11. Cannon, R.L. Segmentation of a thematic Mapper Image Using the Fuzzy C-Means Clustering Algorithm / R.L. Cannon, J.V. Dave, J.C. Bezdek, H.G. Kolsky // IEEE Transactions on Geoscience and Remote Sensing. – V. GE-24, № 3. – P. 400–408.
12. Morlini, I. A New Class of Weighted Similarity Indices Using Polytomous Variables / I. Morlini, S. Zani // Journal of Classification. – 2012. – V. 29, № 2. – P. 199–226. doi: 10.1007 / s00357-012-9107-2.
13. Giordani, P. FINDCLUS: Fuzzy INDividual Differences CLUStering / P. Giordani, H. Kiers // Journal of Classification. – 2012. – V. 29, № 2. – P. 170–198. doi: 10.1007 / s00357-012-9109-0.
14. Contreras, P. Fast, Linear Time Hierarchical Clustering Using the Baire Metric / P. Contreras, F. Murtagh // Journal of Classification. – 2012. – V. 29, № 2. – P. 118–143. doi: 10.1007 / s00357-012-9106-3.
15. Bar-Hen, A. Influence Measures for CART Classification Trees / A. Bar-Hen, S. Gey, J.M. Poggi // Journal of Classification. – 2015. – V. 32, № 1. – P. 21–45. doi: 10.1007/s00357-015-9172-4.
16. Шестаков, А.Л. О новой концепции белого шума / А.Л. Шестаков, Г.А. Свиридюк // Обозрение прикладной и промышленной математики. – 2012. – Т. 19, № 2. – С. 287–288.
17. Шестаков, А.Л. Динамические измерения в пространствах «шумов» / А.Л. Шестаков, Г.А. Свиридюк, Ю.В. Худяков // Вестник Южно-Уральского государственного университета. Серия: Компьютерные технологии, управление, радиоэлектроника. – 2013. – Т. 13, № 2. – С. 4–11.
18. Poynton, C. Rehabilitation of gamma / C. Poynton // Proc. SPIE. – 1998. – V. 1998. – P. 232–242.
19. Stokes, M. A Standard Default Color Space for the Internet / M. Stokes, M. Anderson, S. Chandrasekar, R. Motta. – sRGB. <http://www.w3.org/Graphics/Color/sRGB.html> (запрос 6 декабря 2016)
20. Гонсалес, Р. Цифровая обработка изображений / Р. Гонсалес, Р. Вудс. – М.: Техносфера, 2005.
21. Шапиро, Л. Компьютерное зрение / Л. Шапиро, Дж. Стокман. – М.: БИНОМ. Лаборатория знаний, 2006.

22. Прэрт, У. Цифровая обработка изображений / У. Прэрт. – М.: Мир, 1982.
23. Otsu, N.A. Threshold Selection Method from Gray-Level Histograms / N.A. Otsu // IEEE Trans-Actions on Systems, Man, and Cybernetics. – 1979. – V. 9, № 1. – P. 62–66.
24. Ridler, T.W. Picture Thresholding Using an Iterative Selection Method / T.W. Ridler, S. Calvard // IEEE Trans. System, Man and Cybernetics. – 1978. – V. 8, № 8. – P. 630–632.

*Посохов Иван Александрович, кафедра вычислительной техники и программирования, Магнитогорский государственный технический университет им. Г.И. Носова (г. Магнитогорск, Челябинская область, Российская Федерация), posohoff@bk.ru.*

*Логунова Оксана Сергеевна, доктор технических наук, профессор, кафедра вычислительной техники и программирования, Магнитогорский государственный технический университет им. Г.И. Носова (г. Магнитогорск, Челябинская область, Российская Федерация), logunova66@gmail.com.*

*Миков Анатолий Юрьевич, кафедра вычислительной техники и программирования, Магнитогорский государственный технический университет им. Г.И. Носова (г. Магнитогорск, Челябинская область, Российская Федерация), mikov.ayu@gmail.com.*

*Поступила в редакцию 29 ноября 2016 г.*